Journal of Energy Storage 73 (2023) 109156

Contents lists available at ScienceDirect

Journal of Energy Storage

journal homepage: www.elsevier.com/locate/est

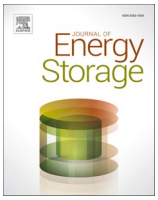

Research papers

Designing thermal regulation materials: Investigating alkylamine length in polymorphic layered hybrid organic-inorganic perovskites

R. Salgado-Pizarro, A. Svobodova-Sedlackova, A.I. Fernández, C. Barreneche *

Departament de Ciència de Materials i Química Física, Secció de Ciència de Materials, Facultat de Química, Universitat de Barcelona, C/Martí i Franquès 1-11, 08028 Barcelona, Spain

ARTICLE INFO

Keywords:
Layered Hybrid Organic-Inorganic Perovskites (LHOIP)
Hybrid Organic-Inorganic Material
Energy Storage Material (ESM)
Thermal Energy Storage (TES)
Solid-Solid Phase Change Materials (ss-PCM)
Phase Transition Material

ABSTRACT

Layered hybrid organic-inorganic perovskites have gained interest in the scientific community due to their feasibility of being used as phase transition materials to store energy by their polymorphism transitions. These compounds represent excellent candidates for cooling electronic devices, given that approximately 55 % of electronic device failures or damage is attributed to internal overheating. Here, we synthesized $(C_{12}H_{25}N)_2CuCl_4$, $(C_{14}H_{29}N)_2CuCl_4$, $(C_{16}H_{33}N)_2CuCl_4$, $(C_{12}H_{24}N)_2MnCl_4$, $(C_{14}H_{29}N)_2MnCl_4$ and $(C_{16}H_{33}N)_2MnCl_4$ to evaluate their potential as thermal regulators and to investigate the dependence of their properties on the length of the alkylamine used. The compounds were synthesized by a liquid phase reaction method and the thermal cycling effect was evaluated after 0, 50, 100 and 200 cycles, between 298 K and 333 K. The crystal structure, molecular structure, and thermal properties of the compounds were characterized and compared before and after the thermal cycling. The maximum enthalpy was obtained for the $(C_{16}H_{33}N)_2CuCl_4$ and $(C_{16}H_{33}N)_2MnCl_4$ with 98.1 and 90.5 $J{\cdot}g^{-1}$, respectively. Additionally, all the components were thermally stable up to 200 cycles, with no evidence of structural degradation or thermal properties decreases. Therefore, our results show that these layered hybrid organic-inorganic perovskites could work as effective thermal regulators. By carefully selecting the alkylamine length, it may be possible to optimize their performance further.

1. Introduction

In the modern energy systems, the energy storage materials (ESMs) are critical components that help attending the global energy issues. They play a crucial role in tackling challenges like climate change, rising energy demand, and the shift to renewable sources. ESMs, such as batteries, supercapacitors, and hydrogen storage materials, offer efficient and reliable energy storage solutions [1]. There are various types of ESMs, including batteries, supercapacitors, and thermal energy storage materials, each with its own set of benefits and drawbacks.

Thermal energy storage (TES) is an important technology that attempts the global energy challenge, as it offers a promising solution for efficient and sustainable energy use. There are various types of TES technologies, including sensible heat storage, latent heat storage, and thermochemical storage, each with its advantages and limitations [2–4]. Latent heat storage materials, phase change materials (PCMs), have emerged as promising solution for thermal management in cooling electronics. As electronic devices continue to become more compact and more powerful, it becomes crucial to efficiently manage their heat to ensure reliability and lifetime [5]. CPUs and batteries are the main sources of heat in portable electronic devices, with CPUs producing heat at densities ranging from 50 $kW{\cdot}m^{-2}$ to 1 $MW{\cdot}m^{-2}$ [6]. Internal overheating causes 55 % of electronic device failure or damage [7,8]. Phase change materials (PCMs) provide a way to store and release thermal energy, effectively controlling the temperature of electronic devices. PCMs present significant advantages in cooling electronics applications due to their high energy storage density. Moreover, PCMs can maintain a constant temperature across a wide range of thermal loads, reducing the necessity for additional cooling mechanism. The use of PCMs opens the way for the development of cutting-edge, electronic devices that may be more compact, efficient, and reliable. Conventional solid-liquid PCMs present several inconveniences which limit their use in electronic devices such as corrosion, leakage, and low heat transfer [9,10]. The ideal PCMs for electronics devices would be those based on solid-solid phase transition since they exhibit minimal volume changes, have better thermal conductivity than normal paraffin used in solid-liquid PCMs, and do not have leakage problems [11,12].

There are four main families of solid-solid PCMs or solid-solid phase

* Corresponding author.
E-mail address: c.barreneche@ub.edu (C. Barreneche).

https://doi.org/10.1016/j.est.2023.109156
Received 11 July 2023; Received in revised form 20 September 2023; Accepted 1 October 2023
Available online 11 October 2023

change materials (ss-PCMs) materials: polymeric, inorganic, organics, and organic-inorganic hybrids [13–15]. The organic ss-PCM mainly includes polyalcohol, plastic crystals and organic-salt-based materials, they present a transition between 298 and 463 K with an enthalpy between 15 and 270 $J{\cdot}g^{-1}$ [16–18]. The solid-solid transition in organic ss-PCMs relies on the change from one crystalline arrangement to another while the temperature increases. Similar behaviour happens with some inorganic ss-PCMs, but a magnetic field induces the crystalline transformations, the average transition temperature is from 250 to 988 °C with enthalpies from 34 to 56 $J{\cdot}g^{-1}$, this family includes ceramic and metallic-based materials such as Ni-Mn-Ti or Fe-Co alloys [19,20]. Polymeric ss-PCMs, on the other hand, have a phase transition temperature of 15 to 60 °C and enthalpy of 10 to 252 $J{\cdot}g^{-1}$. The solid-solid transition in polymers could be due to the presence of a macromolecular backbone like lamellar plates in semicrystalline polymers, hyperbranching or crosslinking that will act as a "hard segment", restricting the movement of the "soft segment" (polymer) to avoid reaching the melting state, as happens with poly(ethylene oxide) (PEO), poly (ethylene glycol) (PEG) and polyurethanes (PU) [21–24]. The same happens with the organic-inorganic hybrids ss-PCMs, which are composed of inorganic two-dimensional crystal that acts as a framework, a 'hard segment', for attaching crystallizable organic segment that acts as a 'soft segment' [25–27]. The transition temperature of organic-inorganic hybrids ss-PCMs, especially layered hybrid organic-inorganic perovskites (LHOIP), are between 32 and 160 °C, and the enthalpies are between 62 and 154 $J{\cdot}g^{-1}$ [13,14]. It is noticeable that inorganic and organic-inorganic hybrids ss-PCMs present thermal conductivities higher than those of polymeric and organic ss-PCM. Fig. 1 shows the figure of merits, which illustrates the quantifiable measure of PCM performance described by Shao et al. [26] as the product of density (ρ), latent heat of transformation (ΔH) and thermal conductivity (k_{HT}) in the high temperature phase ($FOM = \rho{\cdot}\Delta H{\cdot}k_{HT}$). It is noticeable that organic-inorganic hybrids ss-PCMs present a better FOM result than the others.

In this study, we present the synthesis and characterization of copper and manganese-based layered hybrid organic-inorganic compounds as ss-PCMs. This study aims to investigate the effect of alkylamine chain length and composition on the thermal properties and energy storage capacity of these materials. We hypothesize that by tuning the alkylamine chain length and composition, we can achieve optimal thermal properties and high energy storage capacity. To validate this hypothesis, a series of copper and manganese-based layered hybrid organic-inorganic ss-PCMs with varying alkylamine chain lengths and compositions were synthesized. A deep characterization of their thermal properties using differential scanning calorimetry (DSC), thermogravimetric analysis (TGA), and X-ray diffraction (XRD) analysis was performed. Additionally, their specific heat capacity and thermal stability were also evaluated.

2. Experimental procedure

2.1. Synthesis procedure

The reactants n-dodecylamine 98 % (N° CAS 124-22-1), n-tetradecylamine 98 % (N° CAS 2016-42-4) and n-hexadecylamine 90 % (N° CAS 143-27-1) were purchased from Acros Organics, copper (II) chloride dehydrated (N° CAS 10125-13-0) and manganese (II) chloride tetrahydrate (N° CAS 13446-34-9) were purchased from VWR international, hydrochloric acid 37 % (N° CAS 7647-01-0) from Labbox and anhydrous methanol (max. 0.003 % H_2O) (N° CAS 67-56-1) from Merck Group. To synthesize the LHOIP solid structure, we employed the following reaction with stoichiometry given by Eq. (1), using a slight excess of HCl,

$$2(R-NH_2)+2HCl+MCl_2 \rightarrow (R-NH_3)_2MCl_4 \quad (1)$$

where M corresponds to the desired cation (Cu or Mn) and R represents the organic components with the desired length ($C_{12}H_{25}$, $C_{14}H_{29}$ or $C_{16}H_{33}$), in an anhydrous methanol medium. The synthesis procedure is the same as that previously reported [33]. The molar stoichiometric amount of each component was added into a round-bottomed flask with 45 mL of anhydrous methanol. While the products were under constant stirring the HCl, dissolved in 5 mL of anhydrous methanol, was added dropwise through the refrigerant. The solution was refluxed for 4 h, at 64 °C under constant stirring. After the reflux step, the solution was poured into a petri dish and let dry for 7 days in a desiccator. The final dried product was ground with an Agatha mortar for further analysis. The scheme of the synthesis route followed is seen in Fig. 2.

The nomenclature used to identify each product was XC_n, where X represent the cation used (Cu or Mn) and n is the length of the amine used (12, 14 or 16).

2.2. Crystal and molecular structure characterization

To evaluate the crystalline structure in front of the amine length X-ray powder diffraction was applied. The measurements were conducted in a PANalytical X'Pert PRO MPD θ/θ powder diffractometer of 240 mm of radius, in a configuration of a convergent beam with a focalizing mirror and a transmission geometry. The samples were sandwiched between polyester mylar films of 3.6 μm thickness and the test was performed with Cu Kα radiation (λ = 1.5418 Å), a voltage of 45 kV and a

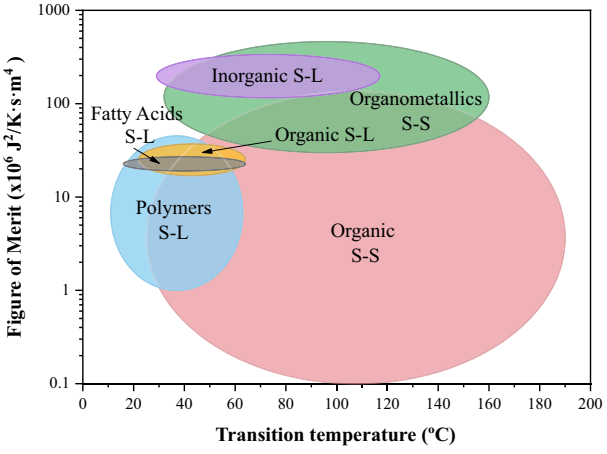

Fig. 1. Figure of Merits vs transition temperature for some PCMs. Data extracted from [13,14,28–32].

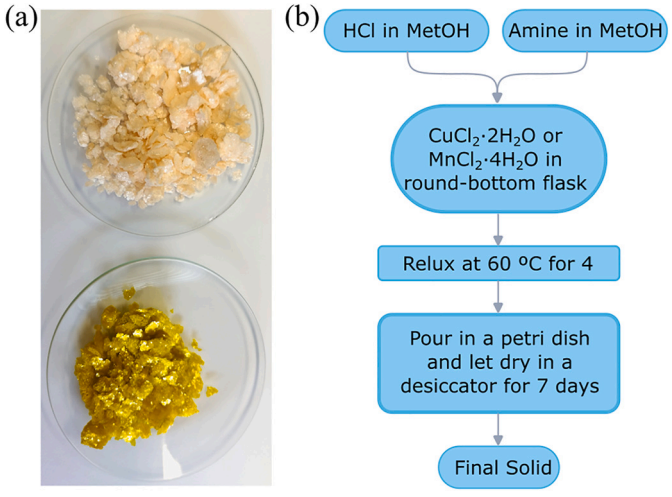

Fig. 2. (a) Images of the solid obtained of Copper and Manganese; (b) Diagram of the synthesis procedure employed.

tube current of 40 mA. The measurements were obtained in continuous scan mode and the 2θ range from 0.5 to 60°2θ with a step size of 0.0263°2θ and a measuring time of 300 s per step.

To determine the molecular structure and to evaluate the chemical change Fourier transformed infrared spectroscopy coupled with Attenuated Total Reflectance (FTIR-ATR) was performed, by using a Spectrum Two from Perkin Elmer. The measurements were conducted with 32 scans over the range of 4000–450 cm^{-1} at a resolution of 4 cm^{-1}.

2.3. Calorimetry study

The effect of amine length and thermal stability was evaluated with a differential scanning calorimeter, DSC 822e Star 3+, from Mettler Toledo. The polymorphic transitions were evaluated with ~2.5 mg which was encapsulated into an Al crucible and a heating ramp from 300 K to 370 K was carried out at 1 $K{\cdot}min^{-1}$.

The specific heat (C_p) was measured at 300, 320, 340, 360 and 380 K following the approach established by Ferrer et al. [34], where the sapphire is analysed as an internal standard and the sample is analysed in successive isothermal segments, without heating ramps and with a temperature difference between the isothermal steps of 1 K. The C_p calculation was made by integrating the heat flow peaks between the isothermal step following the Eq. (2), where C_p is the specific heat, A [$J{\cdot}g^{-1}$] is the integrated area, and the sub-indices s and m correspond to the sapphire (internal standard) and sample, respectively.

$$C_{pm} = \frac{C_{pm} \cdot A_m}{A_s} \tag{2}$$

All the tests performed with the DSC were carried out under 50 mL of nitrogen atmosphere, three measurements per sample were carried out and the average was made discarding the first measurements for the enthalpy and specific heat measurements.

2.4. Thermal cycling stability evaluation

The stability of the layered hybrid compounds was evaluated after 50, 100, and 200 thermal cycles from room temperature to 373 K at 4 $K{\cdot}min^{-1}$, performed with a thermal cycler Q T-18 from Bioer Gene.

3. Results and discussion

3.1. Crystal and molecular structure

The XRD patterns of Cu and Mn components are presented in Fig. 3 (a). It is known that LOIPs presents a two-dimensional structure of alternate staking of alkylammonium and perovskite layers [35]. Clearly, this structure is observed in Fig. 3 (a) where a layered structure is obtained in all the cases due to the observation of diffraction peaks at angles ~6°, 9°, 12°, etc., which corresponds to the (00l) plane perpendicular to the c-axis, which corresponds to the distance between $(XCl_4)^{2-}$ layers [36–40]. The layered structure is formed by alternate staking of $(XCl_4)^{2-}$ and the organic part $2(R\text{-}NH_3)^{1+}$, hence the interlayer distance, d, is in direct dependence on the organic part [41,42]. Also, it is observed a shift to lower angles by the increase of the amine length, and in general, the Mn compound diffraction peaks are detected in lower angles, this is due to the size differences between Cu and Mn.

A triclinic ($P\bar{1}$) system for each ss-PCM was obtained after refinements of the powder patterns profile using FullProf (profile matching), where the crystal parameters (cell parameters) are obtained and presented in Table 1. Furthermore, the results reveal differences in the cell parameters (a, b and c) and therefore in the cell volume. Notice that cell parameter c corresponds to the interlayer distance, (d) [43,44]. A clear trend is observed, whereby longer alkylamine corresponds to larger cell volumes and increases in interlayer distance. The relationship between the interlayer spacing and the number of carbon atoms (n) is depicted in Fig. 3 (b). The interlayer spacing increases with an increase in the alkyl chain length of the amine and shows a linear dependence between d and n (Pearson's R: $R_{CuCn} = 0.99954$ and $R_{MnCn} = 0.99985$), that is in good agreement with the literature [44–46]. Otherwise, the slope of the linear regression of the interlayer distance (d) as a function of the carbon number (n) could be an estimator for the tilt angle [47]. When the chain length increases the chains move from a tilted orientation into the perpendicular direction, therefore, chain tilt decrease with the basal spacing increase. A decreasing chain tilt is indicated by the linear regression slope when it increments exceeding 1.27 Å corresponding to the monolayer packing of alkyl chains per CH_2 unit, that is the case of both CuC_n and MnC_n systems, Fig. 3 (b) [47].

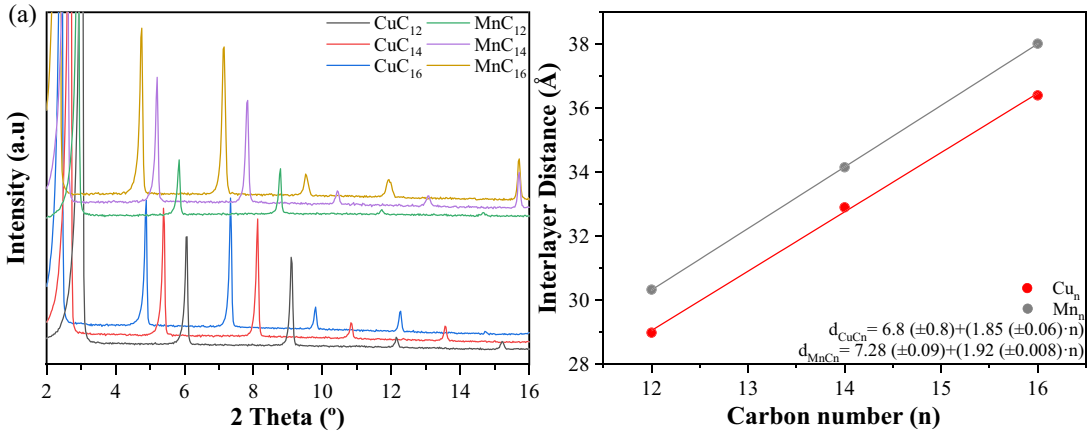

Fig. 3. (a) XRD spectra of the synthesized compound; (b) Interlayer spacing, d (Å), as a function of the number of carbon atoms in the alkylamine, n.

Table 1
ss-PCMs direct cell parameters (a, b, and c in Å) and direct volume cells ($Å^3$) for CuC_n and MnC_n with 12, 14 and 16 carbon atoms in the alkylamine length.

Carbon number, n	CuC_n				MnC_n			
	a (Å)	b (Å)	c (Å)	Direct volume cell ($Å^3$)	a (Å)	b (Å)	c (Å)	Direct volume cell ($Å^3$)
12	5.3468	5.3361	28.9919	808.56	30.3348	4.8634	5.1562	755.42
14	5.3353	5.3358	32.9050	907.92	34.1556	5.1853	5.2398	906.94
16	5.9672	6.0804	36.4016	1138.07	38.0183	5.7652	5.2494	1101.86

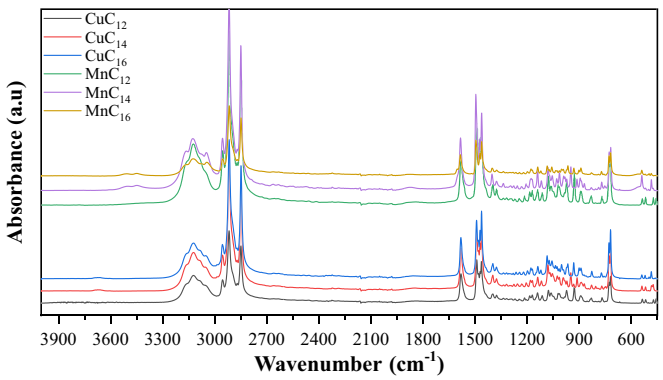

Fig. 4. Infrared spectra of the synthesized compound.

Similar profiles are obtained for the Cu and Mn components in the FTIR-ATR spectra in Fig. 4, showing the main vibration bands of the organic part. The vibrations corresponding to the carbon chain are 2955, 2871, 2917 and 2849 cm^{-1} bands that are the asymmetric and symmetric stretching of R—CH_3 and R—CH_2—R, respectively [36,48]. The 1472 and 1463 cm^{-1} bands are related to the bending of R-CH_2-R. The band at 1377 cm^{-1} is assigned to the symmetrical bending of R—CH_3. The 728 and 720 cm^{-1} bands of R—CH_2—R rocking and 891 cm^{-1} bands of terminal C—C stretching [10,36,45,49]. From the primary amine, the main vibration bands are 3400–3250 cm^{-1} assigned to the stretching vibration of N—H, 1581 cm^{-1} assigned to asymmetric deformation of NH_3^+,1491 and 1480 cm^{-1} symmetric deformation of NH_3^+ and 1215 cm^{-1} of C—N stretching and 769 cm^{-1} of NH_3^+ wagging [36,45].

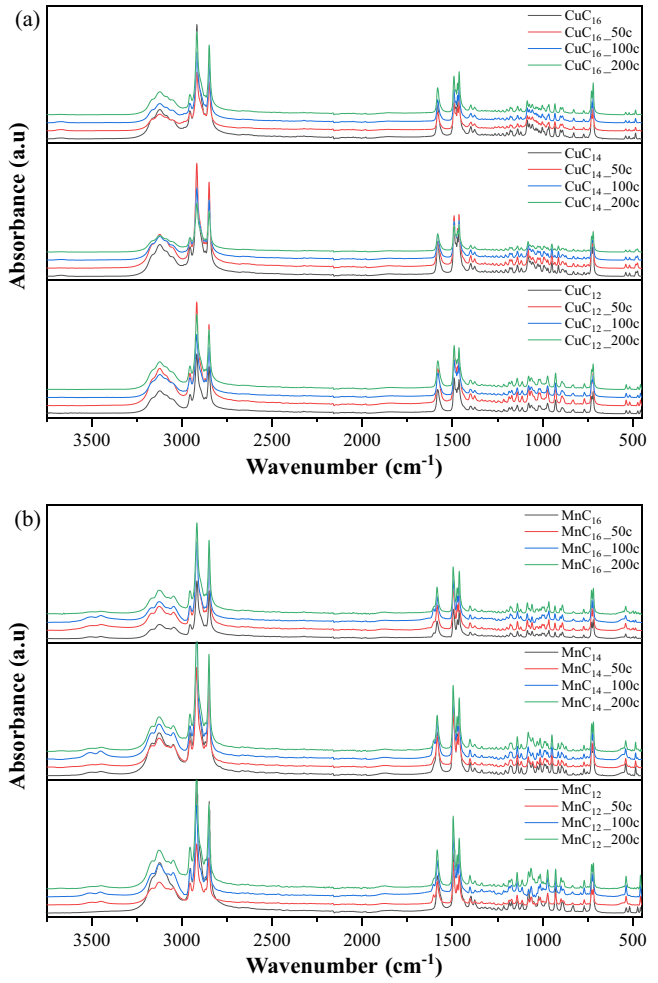

Fig. 5. Infrared spectra of the synthesized compounds over the thermal cycles.

Slight differences between the Cu and Mn compounds are found in FTIR, the 3400–3250 cm^{-1} band assigned to the N—H stretching vibration seems to be shifted to a lower wavenumber in the Mn components however the symmetric and the asymmetric deformation of NH_3^+ are shifted to higher wavenumber values for the Mn components. These differences are related to changes in the polarity of the bonds [50].

The infrared spectra of the thermally cycled samples are displayed in Fig. 5. The analysis reveals that no significant spectral changes occur across the cycles examined. However, for the 100 and 200 cycles cases, we observe differences in absorbance that cannot be attributed to the emergence of new vibrational modes or shifts in existing modes. These changes may stem from a reorganization of the carbon chains within the sample, leading to variations in the amplitudes and frequencies of stretching and bending vibrations.

3.2. Calorimetric study

The heat flow curves from the DSC and the values of transitions from all Cu and Mn components are presented in Table 2 and Fig. 6. Clear differences between materials are observed. The Cu base ss-PCMs present two, three and four transitions, increasing the number with the amine length. The total enthalpy (ΔH), a sum of all the transitions involved in the material, for CuC_{12} is 74.5 $J{\cdot}g^{-1}$, CuC_{14} is 87.1 $J{\cdot}g^{-1}$ and in CuC_{16} is 98.1 $J{\cdot}g^{-1}$. The Mn base ss-PCMs present mainly two transitions, however, it is noticeable that the first transition of MnC16 seems to be two overlapped transitions. The total enthalpy in MnC_{12} is 79.9 $J{\cdot}g^{-1}$, MnC_{14} is 73.5 $J{\cdot}g^{-1}$ and in MnC16 is 90.5 $J{\cdot}g^{-1}$. The values agree with published data [25,45,51–53]. However, it is found that either CuC_{16} as MnC_{16} ss-PCM present an additional transition that is not reported in the literature, this could be due to the method used to synthesize the material since the heating rate for the present study is slower than the applied in [52–54]. The additional transition was found to overlap with those reported, but it is not described like this in the literature [52–54].

As a general behaviour, ss-PCM with a shorter amine length presents lower values of peak temperature (T_p) and lower values of enthalpy. This phenomenon may be related to the energy released during the reorientation of the carbon chain. The longer the amine chain, the higher the energy needed to reorganize the chain [25–27,40].

The stability of the phase transition enthalpy over thermal cycles for all the samples under study was evaluated, see Fig. 7. Small variations of the enthalpy are detected in all the samples, around 7 % taking as a referent the uncycled sample (0 cycles). Those variations may be related to a crystallinity loss or a reorganization of the carbon chain that could affect the enthalpy values. Regarding the peak temperature, no differences were observed.

The specific heat of the samples was measured at temperatures ranging from 300 to 380 K, as shown in Table 3. Although different profiles of specific heat were obtained for each sample, the trends are similar. The specific heat at 340 K in CuC_{14}, CuC_{16}, MnC_{14} and MnC_{16} could not be determined due to its proximity to the polymorphic transition. The highest specific heat values were determined for the samples CuC_{12} and MnC_{12}, with a maximum value of 2.41 $J{\cdot}g^{-1}{\cdot}K^{-1}$ observed in

Table 2
Enthalpy of each transition of the different ss-PCMs.

Transition		CuC_{12}	CuC_{14}	CuC_{16}	MnC_{12}	MnC_{14}	MnC_{16}
1st	ΔH ($J{\cdot}g^{-1}$)	63.2	60.0	66.2[a]	72.5	64.9	77.7[a]
	T_p (K)	330.9	343.6	354.1	331.7	341.3	352.3
2nd	ΔH ($J{\cdot}g^{-1}$)	11.3	9.9	11.3	7.4	8.6	12.8
	T_p (K)	338.1	346.0	358.7	336.0	352.5	370.7
3rd	ΔH ($J{\cdot}g^{-1}$)	–	17.2	20.6	–	–	–
	T_p (K)	–	353.8	365.9	–	–	–

[a] Overlapped transitions.

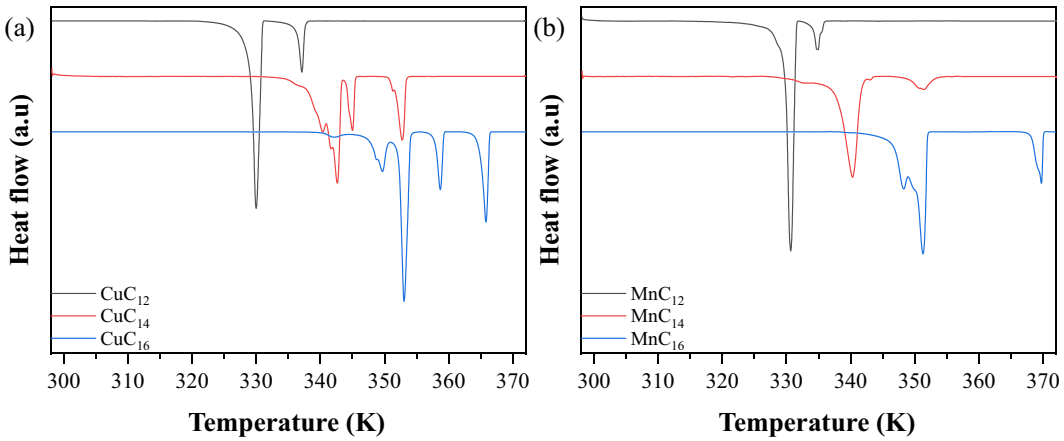

Fig. 6. Heat flow vs temperature profiles of the synthesized compounds: (a) Copper-based samples; (b) Manganese-based samples.

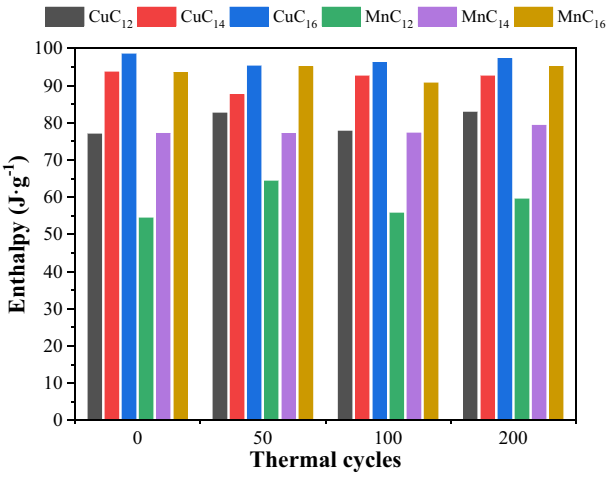

Fig. 7. Enthalpy of the synthesized compounds over the thermal cycles.

Table 3
Specific heat of copper and manganese based samples.

Temperature (K)	Specific heat ($J \cdot g^{-1} \cdot K^{-1}$)					
	CuC_{12}	CuC_{14}	CuC_{16}	MnC_{12}	MnC_{14}	MnC_{16}
300	1.71 ± 0.12	1.47 ± 0.18	1.37 ± 0.05	1.6 ± 0.00	1.60 ± 0.01	1.58 ± 0.01
320	2.41 ± 0.05	2.04 ± 0.03	1.64 ± 0.05	2.38 ± 0.03	1.92 ± 0.00	1.68 ± 0.22
340	1.94 ± 0.02	–	–	1.75 ± 0.01	–	–
360	1.88 ± 0.03	1.97 ± 0.03	2.17 ± 0.10	1.77 ± 0.04	1.97 ± 0.03	2.21 ± 0.02
380	1.95 ± 0.05	2.06 ± 0.06	1.81 ± 0.03	2.84 ± 0.01	1.93 ± 0.04	2.01 ± 0.00

the CuC_{12} sample at 320 K. Regarding the extreme values of 300 and 380 K, a clear trend was observed where the specific heat decreased with increasing alkylamine length. This observation is consistent with the higher organic behaviour of the sample with a larger alkylamine part, resulting in lower specific heat.

4. Conclusions

The dependence of the alkylamine length of LOIPs has been studied in this study. The crystal structure analysis shows a strong dependence on the alkylamine length, increasing the interlayer distance and the volume of the cell by increasing the number of carbons of the alkylamine. The thermo-cycled samples did not show any effect on the crystal and molecular structure. The enthalpy associated with the polymorphic transitions also depends on the alkylamine length. However, the specific heat exhibits an inverse dependence, since the longer the alkylamine chain the lower the specific heat.

These findings provide valuable insights in terms of the structural and thermal behaviour of the present LOIP materials and can be useful in the design of specific PCM with tailored thermal properties. Also, these compounds hold great potential for applications in electronic devices and other fields where temperature regulation is critical, and liquids are incompatible. However, further investigations of materials compatibility and shaping must be done.

CRediT authorship contribution statement

R. Salgado: Conceptualization, Methodology, Formal analysis, Investigation, Data curation, Writing - original draft, Writing - review & editing, Visualization. **A. Svobodova-Sedlackova:** Formal analysis, Investigation, Data curation, Writing - original draft. **C. Barreneche:** Supervision, Review & editing, Funding acquisition. **A. I. Fernández:** Conceptualization, Supervision, Visualization, Review & editing, Funding acquisition.

Declaration of competing interest

The authors declare that they have no known competing financial interests or personal relationships that could have appeared to influence the work reported in this paper.

Data availability

Data will be made available on request.

Acknowledgements

The authors would like to thank the Catalan Government for the quality accreditation given to their research group DIOPMA (2021 SGR 00708). DIOPMA is a certified agent TECNIO in the category of technology developers from the Government of Catalonia. The authors are grateful to the CCiTUB for the assistance with XRD measurements.

This work is partially supported by the grant RTI2018-093849-B-C32 and PID2021-123511OB-C32 funded by MCIN/AEI/10.13039/501100011033 and, as appropriate, by "ERDF A way of making Europe" and the PhD grant PRE2019-087336 funded by MCIN/AEI/10.13039/501100011033 and, as appropriate, by "ESF Investing in your future" of R. Salgado-Pizarro.

References

[1] International Energy Agency (IEA), ETP 2020, 2020.
[2] B. Koçak, A.I. Fernandez, H. Paksoy, Review on sensible thermal energy storage for industrial solar applications and sustainability aspects, Sol. Energy 209 (2020) 135–169, https://doi.org/10.1016/j.solener.2020.08.081.
[3] R. Salgado-Pizarro, A. Calderón, A. Svobodova-Sedlackova, A.I. Fernández, C. Barreneche, The relevance of thermochemical energy storage in the last two decades: the analysis of research evolution, J. Energy Storage 51 (2022) 104377, https://doi.org/10.1016/J.EST.2022.104377.
[4] S.N. Gunasekara, C. Barreneche, A. Inés Fernández, A. Calderón, R. Ravotti, A. Ristić, P. Weinberger, H. Ömur Paksoy, B. Koçak, C. Rathgeber, J. Ningwei Chiu, A. Stamatiou, Thermal Energy Storage Materials (TESMs)—what does it take to make them fly? Crystals (Basel) 11 (2021) 1276, https://doi.org/10.3390/cryst11111276.
[5] P.K. Schelling, L. Shi, K.E. Goodson, Managing heat for electronics, Mater. Today 8 (2005) 30–35, https://doi.org/10.1016/S1369-7021(05)70935-4.
[6] A. Danowitz, K. Kelley, J. Mao, J.P. Stevenson, M. Horowitz, CPU DB, Commun. ACM 55 (2012) 55–63, https://doi.org/10.1145/2133806.2133822.
[7] M. Ikhlaq, M. Yasir, M. Demiroglu, M. Arik, Synthetic jet cooling technology for electronics thermal management - a critical review, IEEE Trans. Compon. Packaging Manuf. Technol. 11 (2021) 1156–1170, https://doi.org/10.1109/TCPMT.2021.3087829.
[8] L.T. Yeh, Review of heat transfer technologies in electronic equipment, J. Electron. Packag. 117 (1995) 333–339, https://doi.org/10.1115/1.2792113.
[9] N. Putra, S. Rawi, M. Amin, E. Kusrini, E.A. Kosasih, T.M. Indra Mahlia, Preparation of beeswax/multi-walled carbon nanotubes as novel shape-stable nanocomposite phase-change material for thermal energy storage, J. Energy Storage 21 (2019) 32–39, https://doi.org/10.1016/j.est.2018.11.007.
[10] R. Salgado-Pizarro, J.A. Padilla, E. Xuriguera, C. Barreneche, A.I. Fernández, Novel shape-stabilized phase change material with cascade character: synthesis, performance and shaping evaluation, Energies (Basel) 14 (2021) 2621, https://doi.org/10.3390/en14092621.
[11] V. Busico, P. Corradini, M. Vacatello, F. Fittipaldi, L. Nicolais, Solid-solid phase transitions for thermal energy storage, in: C. den Duden (Ed.), Thermal Storage of Solar Energy, Springer Netherlands, Dordrecht, 1981, pp. 309–324, https://doi.org/10.1007/978-94-009-8302-1_30.
[12] R. Salgado-Pizarro, M. Martín, A. Svobodova-Sedlackova, A. Calderón, L. Haurie, A.I. Fernández, C. Barreneche, Manufacturing of nano-enhanced shape stabilized phase change materials with montmorillonite by Banbury oval rotor mixer for buildings applications, J. Energy Storage 55 (2022) 105289, https://doi.org/10.1016/J.EST.2022.105289.
[13] A. Fallahi, G. Guldentops, M. Tao, S. Granados-Focil, S. Van Dessel, Review on solid-solid phase change materials for thermal energy storage: molecular structure and thermal properties, Appl. Therm. Eng. 127 (2017) 1427–1441, https://doi.org/10.1016/j.applthermaleng.2017.08.161.
[14] A. Usman, F. Xiong, W. Aftab, M. Qin, R. Zou, Emerging solid-to-solid phase-change materials for thermal-energy harvesting, storage, and utilization, Adv. Mater. 34 (2022) 2202457, https://doi.org/10.1002/adma.202202457.
[15] B. Saparov, D.B. Mitzi, Organic–inorganic perovskites: structural versatility for functional materials design, Chem. Rev. 116 (2016) 4558–4596, https://doi.org/10.1021/acs.chemrev.5b00715.
[16] A. Serrano, M. Duran, J.L. Dauvergne, S. Doppiu, E.P. Del Barrio, Tailored transition temperature plastic crystals with enhanced thermal energy storage capacity, Sol. Energy Mater. Sol. Cells 220 (2021) 110848, https://doi.org/10.1016/J.SOLMAT.2020.110848.
[17] H. Singh, A. Talekar, W.M. Chien, R. Shi, D. Chandra, A. Mishra, M. Tirumala, D. J. Nelson, Continuous solid-state phase transitions in energy storage materials with orientational disorder – computational and experimental approach, Energy. 91 (2015) 334–349, https://doi.org/10.1016/J.ENERGY.2015.07.130.
[18] J. Timmermans, Plastic crystals: a historical review, J. Phys. Chem. Solid 18 (1961) 1–8, https://doi.org/10.1016/0022-3697(61)90076-2.
[19] S. Li, L. He, H. Lu, J. Hao, D. Wang, F. Shen, C. Song, G. Liu, P. Du, Y. Wang, D. Cong, Ultrahigh-performance solid-solid phase change material for efficient, high-temperature thermal energy storage, Acta Mater. 249 (2023) 118852, https://doi.org/10.1016/J.ACTAMAT.2023.118852.
[20] K. Nishioka, N. Suura, K.I. Ohno, T. Maeda, M. Shimizu, Development of Fe base phase change materials for high temperature using solid–solid transformation, ISIJ Int. 50 (2010) 1240–1244, https://doi.org/10.2355/ISIJINTERNATIONAL.50.1240.
[21] H.P. Garg, S.C. Mullick, A.K. Bhargava, Latent heat or phase change thermal energy storage, in: Solar Thermal Energy Storage, Springer Netherlands, Dordrecht, 1985, pp. 154–291, https://doi.org/10.1007/978-94-009-5301-7_3.
[22] Y. Ahmadi, K.-H. Kim, S. Kim, M. Tabatabaei, Recent advances in polyurethanes as efficient media for thermal energy storage, Energy Storage Mater. 30 (2020) 74–86, https://doi.org/10.1016/J.ENSM.2020.05.003.
[23] X. Fu, Y. Xiao, K. Hu, J. Wang, J. Lei, C. Zhou, Thermosetting solid–solid phase change materials composed of poly(ethylene glycol)-based two components: flexible application for thermal energy storage, Chem. Eng. J. 291 (2016) 138–148, https://doi.org/10.1016/J.CEJ.2016.01.096.
[24] J. Zhou, G. Liu, Z. Niu, X. Li, J. Zhao, X. Li, Hyperbranched waterborne polyurethane solid–solid phase change material for thermal energy storage in thermal management fabric, Fibers Polym. 24 (2023) 413–422, https://doi.org/10.1007/S12221-023-00081-3/FIGURES/11.
[25] V. Busico, C. Carfagna, V. Salerno, M. Vacatello, F. Fittipaldi, The layer perovskites as thermal energy storage systems, Solar Energy 24 (1980) 575–579, https://doi.org/10.1016/0038-092X(80)90356-4.
[26] C.R. Raj, S. Suresh, R.R. Bhavsar, V.K. Singh, A.S. Reddy, A. Upadhyay, Manganese-based layered perovskite solid–solid phase change material: synthesis, characterization and thermal stability study, Mech. Mater. 135 (2019) 88–97, https://doi.org/10.1016/j.mechmat.2019.05.004.
[27] D. Li, X.M. Zhao, H.X. Zhao, L.S. Long, L.S. Zheng, Coexistence of magnetic-optic-electric triple switching and thermal energy storage in a multifunctional plastic crystal of trimethylchloromethyl ammonium tetrachloroferrate(III), Inorg. Chem. 58 (2019) 655–662, https://doi.org/10.1021/ACS.INORGCHEM.8B02835/SUPPL_FILE/IC8B02835_SI_001.PDF.
[28] C.R. Raj, S. Suresh, R.R. Bhavsar, V.K. Singh, Recent developments in thermo-physical property enhancement and applications of solid solid phase change materials, J. Therm. Anal. Calorim. 139 (2020) 3023–3049, https://doi.org/10.1007/s10973-019-08703-w.
[29] L. Shao, A. Raghavan, G.H. Kim, L. Emurian, J. Rosen, M.C. Papaefthymiou, T. F. Wenisch, M.M.K. Martin, K.P. Pipe, Figure-of-merit for phase-change materials used in thermal management, Int. J. Heat Mass Transf. 101 (2016) 764–771, https://doi.org/10.1016/j.ijheatmasstransfer.2016.05.040.
[30] M. Irfan Lone, R. Jilte, A review on phase change materials for different applications, Mater. Today Proc. 46 (2021) 10980–10986, https://doi.org/10.1016/j.matpr.2021.02.050.
[31] M.M. Farid, A.M. Khudhair, S.A.K. Razack, S. Al-Hallaj, A review on phase change energy storage: materials and applications, Energ. Conver. Manage. 45 (2004) 1597–1615, https://doi.org/10.1016/j.enconman.2003.09.015.
[32] A. Sharma, V.V. Tyagi, C.R. Chen, D. Buddhi, Review on thermal energy storage with phase change materials and applications, Renew. Sustain. Energy Rev. 13 (2009) 318–345, https://doi.org/10.1016/j.rser.2007.10.005.
[33] R. Salgado-Pizarro, C. Barreneche, A.I. Fernández, Synthesis optimisation of copper-based layered perovskites as thermal energy storage materials, Mater. Today Chem. 30 (2023) 101491, https://doi.org/10.1016/j.mtchem.2023.101491.
[34] G. Ferrer, C. Barreneche, A. Solé, I. Martorell, L.F. Cabeza, New proposed methodology for specific heat capacity determination of materials for thermal energy storage (TES) by DSC, J. Energy Storage. 11 (2017) 1–6, https://doi.org/10.1016/j.est.2017.02.002.
[35] M. Bochalya, S. Kumar, Magnetocaloric effect in 2D-alkylammonium copper halides layered inorganic-organic systems, J. Appl. Phys. 127 (2020) 0–8, https://doi.org/10.1063/1.5134102.
[36] M. Bochalya, P.K. Kanaujia, G. Vijaya Prakash, S. Kumar, Structural and optical diversity in copper halide-based ferromagnetic inorganic-organic layered hybrids, J. Solid State Chem. 273 (2019) 219–225, https://doi.org/10.1016/j.jssc.2019.03.012.
[37] D. He, Y. Di, Y. Yao, Y. Liu, W. Dan, Crystal structure, low-temperature heat capacities, and thermodynamic properties of bis(dodecylammonium) tetrachlorocuprate $(C_{12}H_{28}N)_2CuCl_4$ (s), J. Chem. Eng. Data 55 (2010) 5739–5744, https://doi.org/10.1021/je100699g.
[38] M. Bochalya, G.V. Prakash, S. Kumar, Magnetism and phase segregation in two-dimensional inorganic-organic $(C_{12}H_{25}NH_3)_2Cu_{1-y}Mn_yCl_4$ hybrids, J. Solid State Chem. 273 (2019) 32–36, https://doi.org/10.1016/j.jssc.2019.02.025.
[39] M. Bochalya, P.K. Kanaujia, G.V. Prakash, S. Kumar, Structural phase transitions and thermal stability in Cu-based 2D inorganic-organic hybrid perovskite systems, in: AIP Conf Proc, American Institute of Physics Inc., 2019, p. 030001, https://doi.org/10.1063/1.5122329.
[40] D.B. Mitzi, Synthesis, Structure, and Properties of Organic-Inorganic Perovskites and Related Materials, 2007, pp. 1–121, https://doi.org/10.1002/9780470166499.ch1.
[41] W.W. Zhong, Y.Y. Di, Y.X. Kong, D.F. Lu, J.M. Dou, Lattice potential energies and thermochemical properties of phase change materials (1-CnH2n+1NH 3)2MnCl4 (s) (n = 10 and 11), J. Chem. Thermodyn. 72 (2014) 100–107, https://doi.org/10.1016/j.jct.2014.01.009.
[42] D.H. He, Y.Y. Di, Z.C. Tan, F.F. Yi, W.Y. Dan, Y.P. Liu, Crystal structures and thermochemistry on phase change materials (n-C nH2n1NH3)2CuCl4(s) (n=14 and 15), Solar Energy Mater. Solar Cells 95 (2011) 2897–2906, https://doi.org/10.1016/j.solmat.2011.06.014.
[43] Y. Takeoka, K. Asai, M. Rikukawa, K. Sanui, Systematic studies on chain lengths, halide species, and well thicknesses for lead halide layered perovskite thin films, Bull. Chem. Soc. Jpn. 79 (2006) 1607–1613, https://doi.org/10.1246/bcsj.79.1607.
[44] N. Kitazawa, M. Aono, Y. Watanabe, Excitons in organic–inorganic hybrid compounds (CnH2n+1NH3)2PbBr4 (n=4, 5, 7 and 12), Thin Solid Films 518 (2010) 3199–3203, https://doi.org/10.1016/j.tsf.2009.09.014.
[45] J.-K. Kang, J.-H. Choy, M. Rey-Lafon, Phase transition behavior in the perovskite-type layer compound $(n\text{-}C_{12}H_{25}NH_3)_2CuCl_4$, J. Phys. Chem. Solid 54 (1993) 1567–1577, https://doi.org/10.1016/0022-3697(93)90351-Q.
[46] Y. Fukuta, T. Miyata, Y. Hamanaka, Fabrication of two-dimensional hybrid organic–inorganic lead halide perovskites with controlled multilayer structures by liquid-phase laser ablation, J. Mater. Chem. C Mater. 11 (2023) 910–916, https://doi.org/10.1039/D2TC04395E.
[47] G. Lagaly, Interaction of alkylamines with different types of layered compounds, Solid State Ion. 22 (1986) 43–51, https://doi.org/10.1016/0167-2738(86)90057-3.
[48] R. Salgado-Pizarro, G. Ulldemolins, M.E. Navarro, A. Palacios, A. Calderón, Y. Ding, A.I. Fernández, C. Barreneche, New shape-stabilized phase change materials obtained by single-screw extruder, Energy Storage 3 (2021), https://doi.org/10.1002/est2.268.

[49] R.G. Snyder, Vibrational spectra of crystalline n-paraffins, J. Mol. Spectrosc. 7 (1961) 116–144, https://doi.org/10.1016/0022-2852(61)90347-2.
[50] E. Pretsch, T. Clerc, J. Seibl, W. Simon, Tabellen zur Strukturaufklärung organischer Verbindungen mit spektroskopischen Methoden, 1976, p. 15, https://doi.org/10.1007/978-3-662-13076-6.
[51] G.F. Needham, R.D. Willett, H.F. Franzen, Phase transitions in crystalline models of bilayers. 1. Differential scanning calorimetric and x-ray studies of $(C_{12}H_{25}NH_3)_2MCl_4$ and $(C_{14}H_{29}NH_3)_2MCl_4$ salts (M = Mn^{2+}, Cd^{2+}, Cu^{2+}), J. Phys. Chem. 88 (1984) 674–680, https://doi.org/10.1021/j150648a012.
[52] E. Landi, M. Vacatello, Metal-dependent thermal behaviour in (n-$C_nH_{2n+1}NH_3)_2MCl_4$, Thermochim. Acta 13 (1975) 441–447, https://doi.org/10.1016/0040-6031(75)85084-2.
[53] W. Li, D. Zhang, T. Zhang, T. Wang, D. Ruan, D. Xing, H. Li, Study of solid–solid phase change of (n-$C_nH_{2n+1}NH_3)_2MCl_4$ for thermal energy storage, Thermochim. Acta 326 (1999) 183–186, https://doi.org/10.1016/S0040-6031(98)00497-3.
[54] V. Busico, C. Carfagna, V. Salerno, M. Vacatello, Thermal behavior of complexes of general formula (n-$C_nH_{2n+1}NH_2)_2CuCl_2$, Thermochim. Acta 39 (1980) 1–5, https://doi.org/10.1016/0040-6031(80)80051-7.